Hindawi Publishing Corporation
International Journal of Aerospace Engineering
Volume 2015, Article ID 878971, 16 pages
http://dx.doi.org/10.1155/2015/878971

Research Article

Robust Predictive Functional Control for Flight Vehicles Based on Nonlinear Disturbance Observer

Yinhui Zhang, Huabo Yang, Zhenyu Jiang, Fan Hu, and Weihua Zhang

College of Aerospace Science and Engineering, National University of Defense Technology, Changsha 410073, China

Correspondence should be addressed to Yinhui Zhang; zhangyinhui_nudt@163.com

Received 29 March 2015; Revised 12 July 2015; Accepted 14 July 2015

Academic Editor: Ronald M. Barrett

A novel robust predictive functional control based on nonlinear disturbance observer is investigated in order to address the control system design for flight vehicles with significant uncertainties, external disturbances, and measurement noise. Firstly, the nonlinear longitudinal dynamics of the flight vehicle are transformed into linear-like state-space equations with state-dependent coefficient matrices. And then the lumped disturbances are considered in the linear structure predictive model of the predictive functional control to increase the precision of the predictive output and resolve the intractable mismatched disturbance problem. As the lumped disturbances cannot be derived or measured directly, the nonlinear disturbance observer is applied to estimate the lumped disturbances, which are then introduced to the predictive functional control to replace the unknown actual lumped disturbances. Consequently, the robust predictive functional control for the flight vehicle is proposed. Compared with the existing designs, the effectiveness and robustness of the proposed flight control are illustrated and validated in various simulation conditions.

1. Introduction

Flight control system design is a quite acknowledged challenging task, particularly when the flight vehicle is confronted with strong nonlinearity, great uncertainty, external disturbance, and measurement noise [1–4]. Various flight controllers from linear to nonlinear control strategies have been developed during the past decades, such as gain scheduled control [5], LPV control [6], H_∞ control [7], dynamic inversion control [8], sliding model control (SMC) [9, 10], backstepping control [11, 12], and adaptive control [13–15].

In recent years, as one of the analytic model predictive control (MPC) methods, the predictive functional control (PFC) has been deeply investigated and successfully adopted in various industrial applications [16–20]. Whereas an accurate mathematical model to predict the plant output is crucial for the PFC, it may not achieve the satisfactory performance when considering significant uncertainties or external disturbances. In order to improve the accuracy of the predictive model as well as the robustness of the PFC, two potential approaches are worth further studying. The first approach is the model identification, such as recursive fuzzy identification algorithm [21, 22], which focuses on the acquisition of an exact plant model. Meanwhile, the second approach takes advantage of a disturbance observer to estimate the lumped disturbance of the plant model [16, 20] and principally concentrates on the compensation of the predictive model rather than recognizing it to be extremely accurate. Since the former approach is more complex, it is an engineering foresight to introduce the disturbance observer into the PFC.

In order to estimate the disturbance, various disturbance observers have been developed, such as time delay control (TDC) [23], uncertainty and disturbance estimator (UDE) [24], and extended state observer (ESO) [25]. However, the aforementioned two disturbance observers are just restricted to the linear systems, and the ESO is available for the integral-chain nonlinear system but sensitive to the measurement noise. Therefore, Chen [26] designed a nonlinear disturbance observer (NDO), in which the nonlinear observer gains can be designed as linear or nonlinear functions. Compared with the other disturbance observers, the NDO can be applied to numerous types of system models, and the applications can be referred to [27, 28].

When the lumped disturbances are estimated via the disturbance observer, it is easy to compensate the matched disturbances via combining a feedforward compensation part based on disturbance observer and a feedback regulation part based on PFC. However, there are few investigations for the PFC on the compensation of the mismatched disturbance until now. Note that the disturbance-based feedforward control for systems with mismatched disturbances is a longstanding unresolved problem [29, 30]. By appropriately designing a disturbance compensation gain vector, Li et al. [31] and Yang et al. [28] proposed the composite control to deal with the mismatched disturbances for linear and nonlinear systems, respectively. Yang et al. [32] designed a novel sliding surface with the mismatched disturbances and extended the theory and application of the traditional sliding mode control. The former approach seems concise, but the compensation gain vector is complex to design. While the latter approach seems complex, the application for sliding mode control is much more concise. Based on these rules, a novel robust PFC method is proposed based on nonlinear disturbance observer according to the idea of the novel sliding mode control.

The remainder of this paper is organized as follows. In Section 2, the longitudinal model of a generic flight vehicle is presented. Section 3 investigates the theory and application of the proposed NDOEPFC. Comparison results in various simulation conditions with the existing flight controllers are illustrated in Section 4, and the conclusion is given in Section 5.

2. Flight Vehicle Model

The longitudinal dynamic model for a generic flight vehicle is taken from [33], which has been used in numerous studies on the design and analysis of pitch flight control. Considering the parameter uncertainties and external disturbances, the nonlinear dynamic equation of the flight vehicle model with a first-order servo is given as follows:

$$\begin{aligned}
\dot{\alpha} &= \left(1+\Delta f_1\right) f_1(\alpha) + q + \left(1+\Delta b_1\right) b_1(\alpha)\,\delta + \Delta d_1,\\
\dot{q} &= \left(1+\Delta f_2\right) f_2(\alpha) + \left(1+\Delta b_2\right) b_2\delta + \Delta d_2,\\
\dot{\delta} &= \frac{(-\delta+u)}{[(1+\Delta\tau)\,\tau]} + \Delta d_3,
\end{aligned} \tag{1}$$

where α, q, and δ are the angle of attack (deg), pitch rate (deg/s), and rudder deflection (deg), respectively. τ is the time constant of the servo (s). u is the control command (deg). $f_1(\alpha), b_1(\alpha), f_2(\alpha)$, and b_2 are the known components of the dynamic model represented as follows:

$$\begin{aligned}
&f_1(\alpha)\\
&\quad= \frac{180QS}{\pi mV}\left[a_n\alpha^3 + b_n|\alpha|\,\alpha + c_n\left(2-\frac{M}{3}\right)\alpha\right]\cos(\alpha),\\
&b_1(\alpha) = \frac{180QS}{\pi mV} d_n\cos(\alpha),\\
&f_2(\alpha)\\
&\quad= \frac{180QSd}{\pi I_{yy}}\left[a_m\alpha^3 + b_m|\alpha|\,\alpha + c_m\left(-7+\frac{8M}{3}\right)\alpha\right],\\
&b_2 = \frac{180QSd}{\pi I_{yy}} d_m,\\
&Q = \frac{1}{2}\rho V^2,
\end{aligned} \tag{2}$$

where m is the vehicle mass (kg), V is the flight velocity (m/s), M is the flight Mach number, Q is the dynamic pressure (Pa), S and d are the reference area (m^2) and length (m), respectively, I_{yy} is the moment of inertia ($kg.m^2$), and $a_n, b_n, c_n, d_n, a_m, b_m, c_m$, and d_m are the aerodynamic coefficients.

Given the characteristic status of the longitudinal dynamic model at Mach 3 and an altitude of 6096 m, the coefficients of (1) and (2) are listed in Table 1.

The parameters in the nonlinear flight vehicle model, $\Delta f_1, \Delta b_1, \Delta f_2, \Delta b_2$, and $\Delta\tau$, represent the uncertainties of the aerodynamic coefficients and servo time constant, respectively. In addition, $\Delta d_1, \Delta d_2$, and Δd_3 denote the external disturbances resulting from the unmodeled dynamic, wind disturbance, installation error, and unknown servo character.

Table 1: Coefficients of the flight vehicle model.

Coefficient	Value	Unit
a_n	$1.03e-4$	deg^{-3}
b_n	$-9.45e-3$	deg^{-2}
c_n	$-1.7e-1$	deg^{-1}
d_n	$-3.4e-2$	deg^{-1}
S	$4.087e-2$	m^2
τ	0.1	s
m	4410	kg
I_{yy}	247.44	$Kg{\cdot}m^2$
a_m	$2.15e-4$	deg^{-3}
b_m	$-1.95e-2$	deg^{-2}
c_m	$5.1e-2$	deg^{-1}
d_m	$-2.06e-1$	deg^{-1}
d	0.229	m
g	9.8	m/s^2
V	947.6	m/s
ρ	$6.54e-1$	kg/m^3

3. Robust PFC Design

Similar to the other model predictive control (MPC), the predictive functional control (PFC) is designed based on

the exact model. The error correction approach guarantees the PFC with effective and robust performance when taking the model uncertainties and external disturbances into consideration. Owing to the correction of the output predictive error in the PFC, the asymptotically disturbance suppression may be achieved in a relatively slow way, but it is still formidable to attenuate the disturbances to an adequate desired degree within a certain time. To address this challenge, a nonlinear disturbance observer (NDO) is introduced to estimate the lumped disturbances. Thus, the estimated disturbances, as a part of the linear-like state-space equation, are imported into the predictive model of the PFC to improve the predictive precision, which in turn enhances the tracking robust performance of the PFC.

3.1. Robust PFC with Disturbances. In order to enhance the effectiveness and robustness of the PFC, the external disturbances are imported into the predictive model. Hence, the predictive model output of the robust PFC gets more accurate towards the actual system output. Therefore, together with the error correction and performance index optimization, the PFC with disturbances can provide an excellent tracking performance and robustness to model uncertainties and external disturbances.

3.1.1. Predictive Model. First, the combination or total effect of parameter uncertainties and external disturbances, acting on the nonlinear longitudinal model of the flight vehicle, is treated as a lumped disturbance of the system in each dynamic channel as

$$\begin{aligned} d_1 &= \Delta\alpha \cdot f_1(\alpha) + \Delta b_1 \cdot b_1(\alpha)\delta + \Delta d_1, \\ d_2 &= \Delta q \cdot f_2(\alpha) + \Delta b_2 \cdot b_2\delta + \Delta d_2, \\ d_3 &= \frac{(-\delta + u)}{[(1+\Delta\tau)\tau]} - \frac{(-\delta + u)}{\tau + \Delta d_3}. \end{aligned} \tag{3}$$

And then, let $\mathbf{d} = [d_1 \;\; d_2 \;\; d_3]^T$ represent the lumped disturbances. Similar to the SDRE method, the state-space equations of state-dependent coefficients are reconstructed from the nonlinear longitudinal dynamics of the flight vehicle as

$$\begin{aligned} \dot{\mathbf{x}}_m &= \mathbf{A}_m(\mathbf{x}_m)\mathbf{x}_m + \mathbf{B}_m u + \mathbf{d}, \\ y_m &= \mathbf{C}_m \mathbf{x}_m, \end{aligned} \tag{4}$$

where $\mathbf{x}_m$ is the predictive state, y_m is the predictive output, and $\mathbf{A}_m(\mathbf{x}_m)$, $\mathbf{B}_m$, and $\mathbf{C}_m$ are the state-dependent coefficient matrixes described as

$$\begin{aligned} \mathbf{A}_m(\mathbf{x}_m) &= \begin{bmatrix} f_{1\alpha}(\alpha) & 1 & b_1(\alpha) \\ f_{2\alpha}(\alpha) & 0 & b_2 \\ 0 & 0 & -\dfrac{1}{\tau} \end{bmatrix}, \\ \mathbf{B}_m &= \begin{bmatrix} 0 & 0 & \dfrac{1}{\tau} \end{bmatrix}^T, \\ \mathbf{C}_m &= \begin{bmatrix} 1 & 0 & 0 \end{bmatrix}^T, \end{aligned} \tag{5}$$

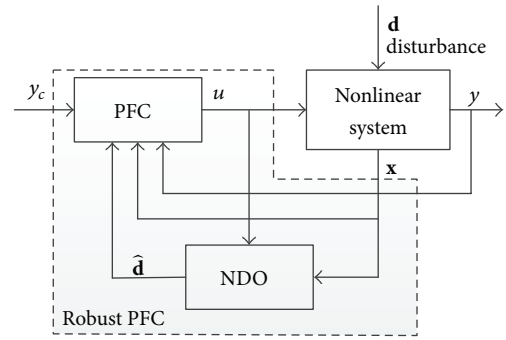

Figure 1: The framework of the robust PFC.

where

$$\begin{aligned} f_1(\alpha) &= f_{1\alpha}(\alpha) \cdot \alpha, \\ f_2(\alpha) &= f_{2\alpha}(\alpha) \cdot \alpha. \end{aligned} \tag{6}$$

By discretizing (4) at each sampling instant, the discrete predictive model of PFC can be acquired as

$$\begin{aligned} \mathbf{x}_m(k+1) &= \mathbf{G}_m \mathbf{x}_m(k) + \mathbf{H}_m u(k) + \mathbf{N}_m \mathbf{d}(k), \\ y_m(k) &= \mathbf{C}_m \mathbf{x}_m(k), \end{aligned} \tag{7}$$

where $\mathbf{G}_m$, $\mathbf{H}_m$, and $\mathbf{N}_m$ are the coefficient matrixes of the discrete predictive model expressed as

$$\begin{aligned} \mathbf{G}_m &= e^{\mathbf{A}_m(\mathbf{x}_m)T_s}, \\ \mathbf{H}_m &= \int_0^{T_s} e^{\mathbf{A}_m(\mathbf{x}_m)T_s} \mathbf{B}_m \mathrm{d}t, \\ \mathbf{N}_m &= \int_0^{T_s} e^{\mathbf{A}_m(\mathbf{x}_m)T_s} \mathbf{I}_{3\times 3} \mathrm{d}t, \end{aligned} \tag{8}$$

where T_s is the discrete period of the predictive model, which is usually equal to the control period.

Remark 1. From (6), we can see that the predictive model of the PFC is just the reconstruction of the system model, and the coefficient matrixes in (5) and (8) can be approximately precalculated offline by regarding the states as a variant parameter.

3.1.2. Control Structure. The control command of the PFC is structured as a linear prespecified combination of base functions:

$$u(k+i) = \sum_{j=1}^{N_b} \mu_j f_j(i), \quad i = 0, 1, \ldots, P-1, \tag{9}$$

where $f_j(\cdot)$ is the selected base functions, μ_j is the weight coefficient corresponding to $f_j(\cdot)$, N_b is the number of the base functions, and P is the prediction horizon. In principle, the choice of the base functions is determined by the form of the reference signals, and the canonical functions are regularly used, for example, step, ramp, and parabola.

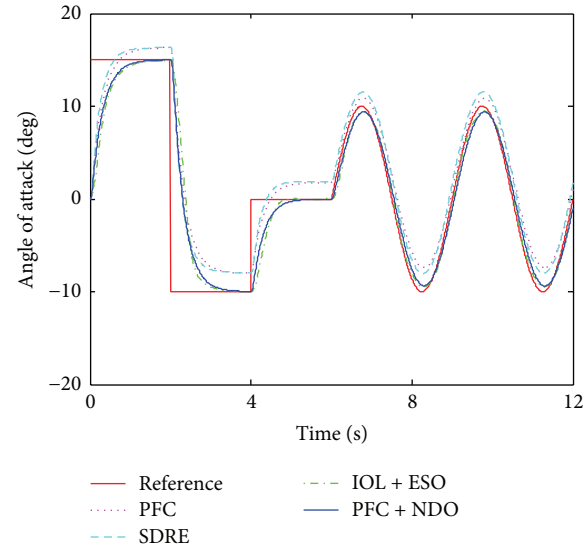

(a) Angle of attack (deg)

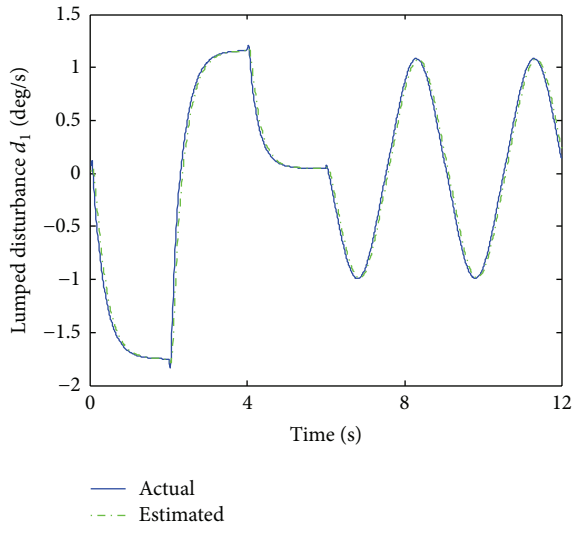

(b) Lumped disturbance d_1 (deg/s)

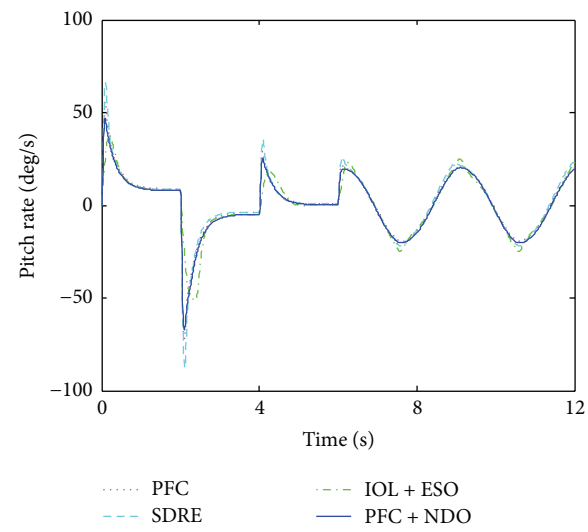

(c) Pitch rate (deg/s)

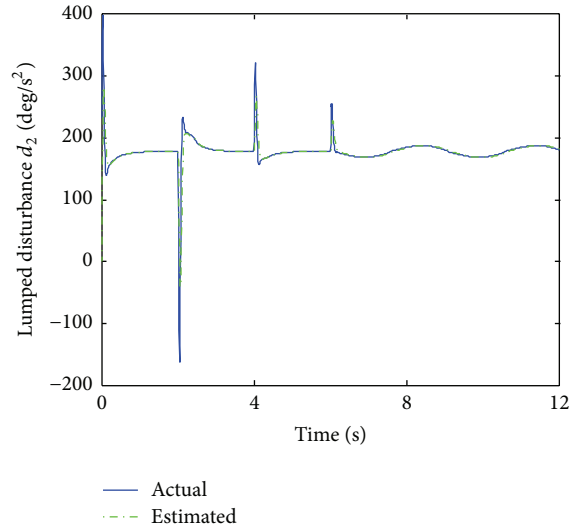

(d) Lumped disturbance d_2 (deg/s^2)

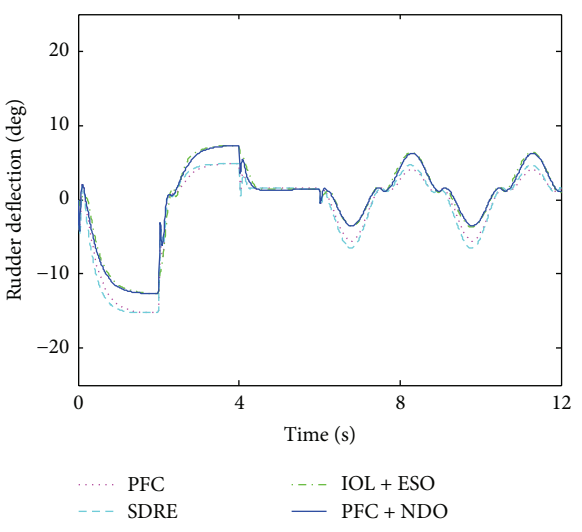

(e) Rudder deflection (deg)

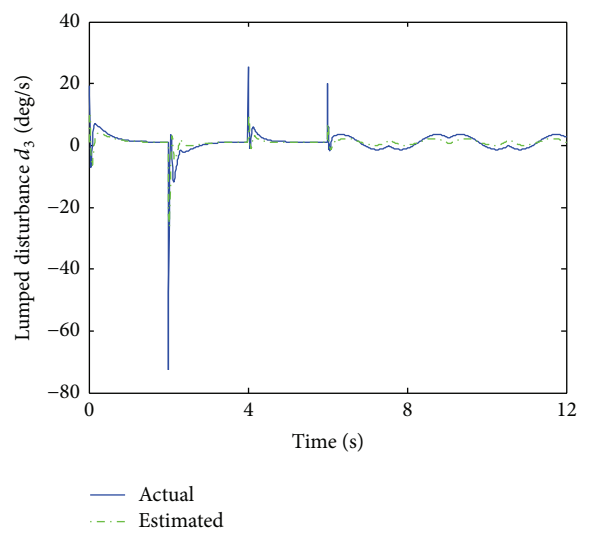

(f) Lumped disturbance d_3 (deg/s)

Figure 2: Continued.

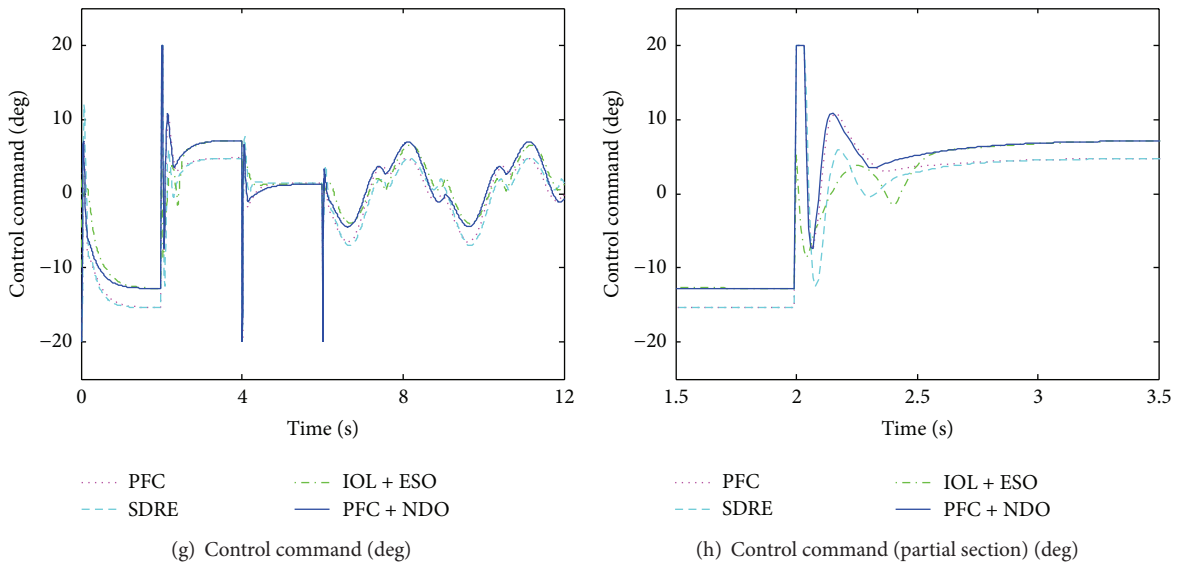

(g) Control command (deg)

(h) Control command (partial section) (deg)

FIGURE 2: Simulation responses under the four controllers and the estimate performance of the NDO in the case of positive uncertainties and disturbances.

3.1.3. Predictive Output. In practice, the lumped disturbance is mainly composed of some signals with little perturbation. Thus, within the prediction horizon, it can be assumed that

$$\mathbf{d}(k+i) \approx \mathbf{d}(k). \tag{10}$$

Substituting (9) and (10) into (7), the predictive output at the time instant $(k+i)$ can then be derived as

$$\begin{aligned} y_m(k+i) = {} & \mathbf{C}_m \mathbf{G}_m^i \mathbf{x}_m(k) + \sum_{l=1}^{N_b} \mu_l \sum_{j=0}^{i-1} \mathbf{C}_m \mathbf{G}_m^{i-1-j} \mathbf{H}_m f_l(j) \\ & + \sum_{j=0}^{i-1} \mathbf{C}_m \mathbf{G}_m^{i-1-j} \mathbf{N}_m \mathbf{d}(k). \end{aligned} \tag{11}$$

3.1.4. Error Correction. Despite the attendant of the lumped disturbance, there are still a few errors between the predictive output and the practical output due to various kinds of uncertainties, noise, and the estimated error. Therefore, given the fact that the predictive output errors within the prediction horizon are equivalent, we get

$$e(k+i) = y(k+i) - y_m(k+i) = y(k) - y_m(k). \tag{12}$$

The actual output prediction is then corrected via the predictive output error to improve the accuracy of the predictive model as

$$y_p(k+i) = y_m(k+i) + e(k+i). \tag{13}$$

3.1.5. Reference Trajectory. Supposing the desired output at the time instant $k+i$ is $y_c(k+i)$, the reference trajectory is defined as

$$y_r(k+i) = y_c(k+i) - \beta^i \left[y_c(k) - y(k) \right], \tag{14}$$

where $y_r(k+i)$ is the reference trajectory at the time instant $k+i$, $\beta = e^{-T_s/T_r}$ is the softness factor, and T_r is the expected settling time of the reference trajectory.

3.1.6. Performance Index. The tracking error is the essential valuation of the flight control; consequently, a quadratic sum of the tracking errors between the actual output prediction and the reference trajectory at several particular instants can be selected as the performance index, given by

$$\begin{aligned} J &= \sum_{h_i \in H_{N_c}} \left[y_p(k+h_i) - y_r(k+h_i) \right]^2 \\ &= \sum_{h_i \in H_{N_c}} \begin{bmatrix} \mathbf{C}_m \mathbf{G}_m^{h_i} \mathbf{x}_m(k) + \boldsymbol{\mu} \cdot \boldsymbol{\theta}(h_i) + \boldsymbol{\eta} \cdot \mathbf{d}(k) + y(k) \\ - y_m(k) - y_c(k+h_i) + \beta^{h_i} y_c(k) - \beta^{h_i} y(k) \end{bmatrix}^2 \\ &= \sum_{h_i \in H_{N_c}} \left[M(h_i) + \boldsymbol{\mu} \cdot \boldsymbol{\theta}(h_i) \right]^2, \end{aligned} \tag{15}$$

where h_i represents the coincidence point belonging to the set of H_{N_c} for a number of N_c, $M(h_i) = \mathbf{C}_m \mathbf{G}_m^{h_i} \mathbf{x}_m(k) + \boldsymbol{\eta} \cdot \mathbf{d}(k) + y(k) - y_m(k) - y_c(k+h_i) + \beta^{h_i} y_c(k) - \beta^{h_i} y(k)$, and

$$\begin{aligned} \boldsymbol{\mu} &= \left[\mu_1, \ldots, \mu_{N_b} \right], \\ \boldsymbol{\theta}(i) &= \left[\theta_1(i), \ldots, \theta_{N_b}(i) \right]^T, \\ \theta_l(i) &= \sum_{j=0}^{i-1} \mathbf{C}_m \mathbf{G}_m^{i-1-j} \mathbf{H}_m f_l(j), \\ \boldsymbol{\eta} &= \sum_{j=0}^{i-1} \mathbf{C}_m \mathbf{G}_m^{i-1-j} \mathbf{N}_m. \end{aligned} \tag{16}$$

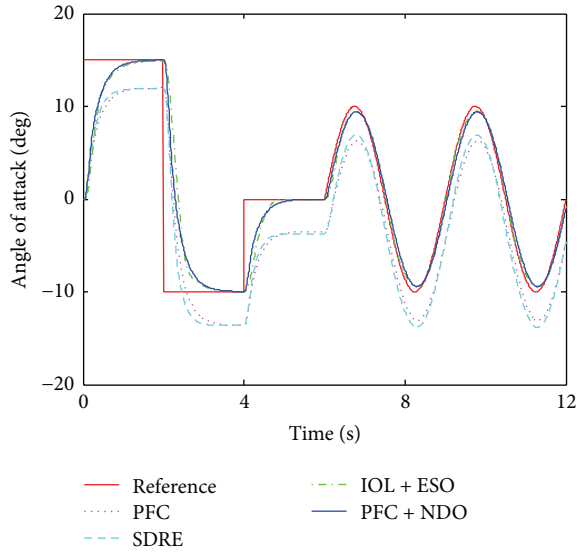

(a) Angle of attack (deg)

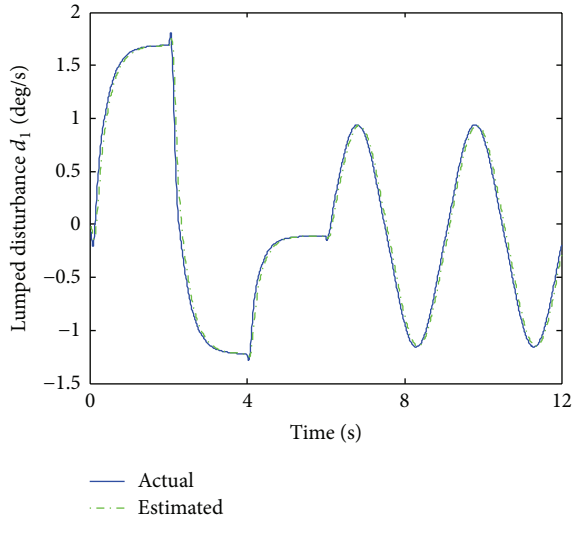

(b) Lumped disturbance d_1 (deg/s)

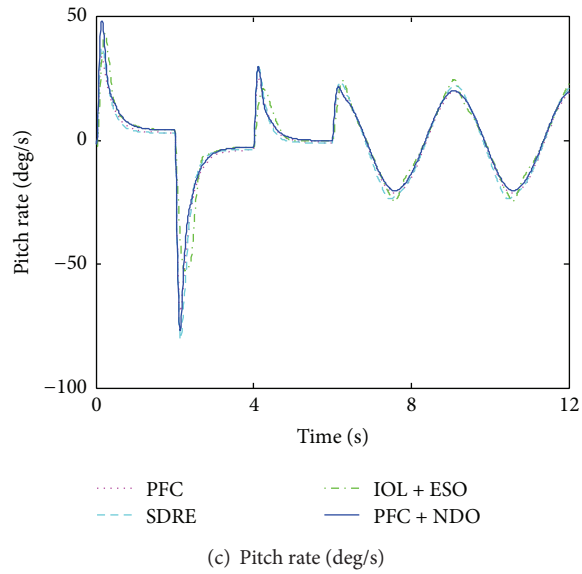

(c) Pitch rate (deg/s)

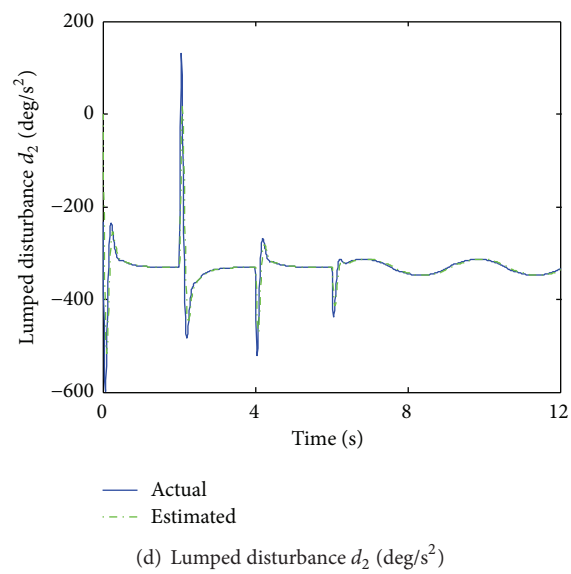

(d) Lumped disturbance d_2 (deg/s^2)

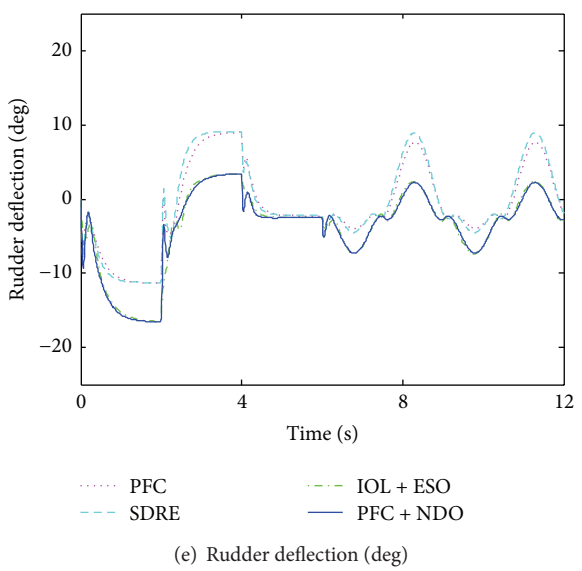

(e) Rudder deflection (deg)

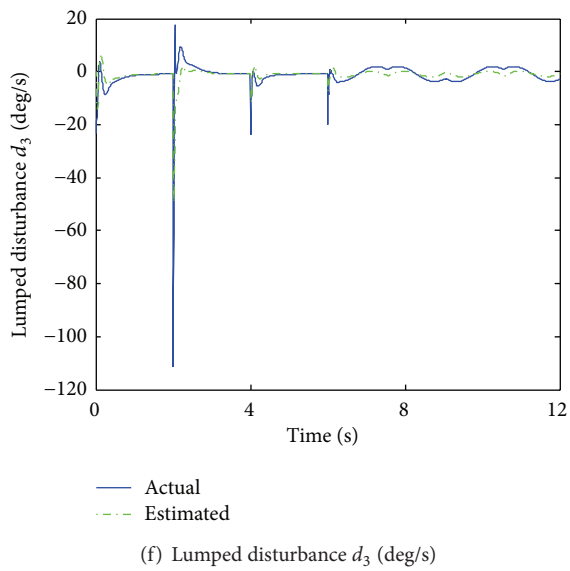

(f) Lumped disturbance d_3 (deg/s)

Figure 3: Continued.

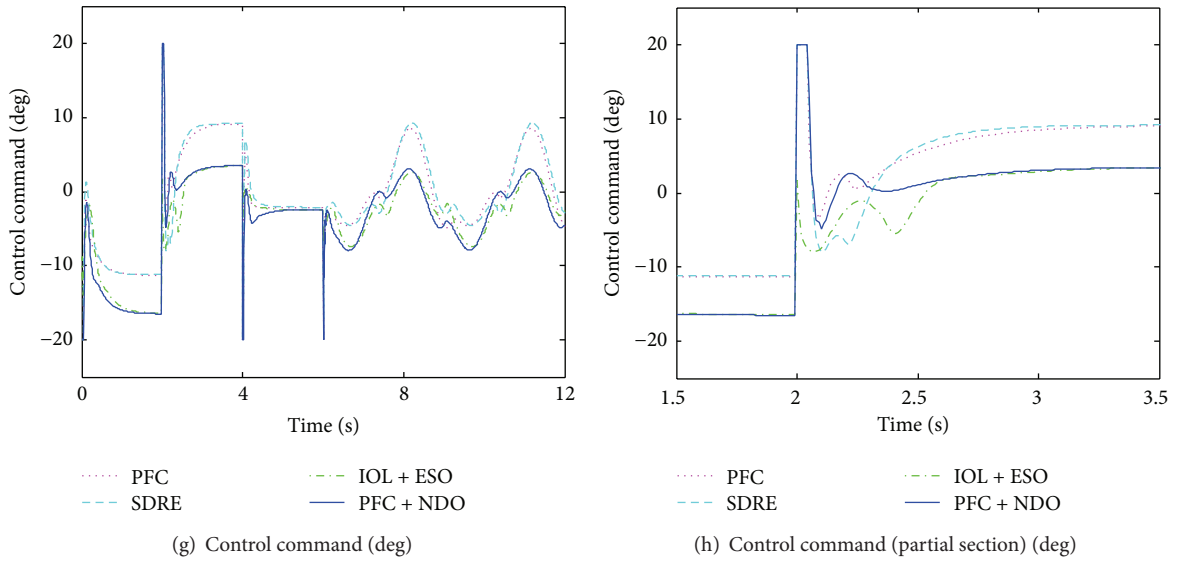

(g) Control command (deg)

(h) Control command (partial section) (deg)

FIGURE 3: Simulation responses under the four controllers and the estimate performance of the NDO in the case of negative uncertainties and disturbances.

3.1.7. Optimal Control. In the case of no constraints, the optimal control can be derived by minimizing the performance index J with respect to the weight coefficient $\boldsymbol{\mu}^T$, depicted as

$$\frac{\mathrm{d}J}{\mathrm{d}\boldsymbol{\mu}^T} = 0. \tag{17}$$

That is,

$$\sum_{h_i \in H_{N_c}} \left[M\left(h_i\right) + \boldsymbol{\mu} \cdot \boldsymbol{\theta}\left(h_i\right)\right] \cdot \boldsymbol{\theta}\left(h_i\right) = 0. \tag{18}$$

Let $\mathbf{M} = [M(h_1), \ldots, M(h_{N_c})]$, $\boldsymbol{\Theta} = [\boldsymbol{\theta}(h_1), \ldots, \boldsymbol{\theta}(h_{N_c})]$; then, (18) can be rewritten as

$$\left(\mathbf{M} + \boldsymbol{\mu}\boldsymbol{\Theta}\right)\boldsymbol{\Theta}^T = 0. \tag{19}$$

Therefore, if the matrix $\boldsymbol{\Theta}\boldsymbol{\Theta}^T$ is reversible, the optimal weight coefficient of the base function can be expressed as

$$\boldsymbol{\mu} = -\mathbf{M}\boldsymbol{\Theta}^T\left(\boldsymbol{\Theta}\boldsymbol{\Theta}^T\right)^{-1}. \tag{20}$$

The optimal control is then given by

$$u\left(k\right) = \boldsymbol{\mu}\mathbf{F}, \tag{21}$$

where $\mathbf{F} = [f_1(0), \ldots, f_{N_b}(0)]^T$.

3.1.8. Problems of Constraint. Up to the present, it is unclear for the PFC to deal with the state and output constraints [34]. Thus, only the control input constraint is considered in this paper. In practice, the control input constraint of the flight vehicle is primarily dependent on the character of the control actuator. Assume that the constraints imposed on the actuator of the flight vehicle are $-20^\circ \le \delta \le 20^\circ$ for its deflection and $-250^\circ/\mathrm{s} \le \dot{\delta} \le 250^\circ/\mathrm{s}$ for its rate of change, respectively. Actually, the constraints of the actuator are inherent self-constraints, and the maximum rate of change relates to the bandwidth of the actuator within minor deflection. Based on this discussion, only the control magnitude is indispensable to be constrained within $[-20^\circ, 20^\circ]$, whereas the rate of the control change is simply determined by the model of the actuator in the predictive model.

3.2. Robust PFC Based on NDO. In practice, due to the complex structure and great uncertainties, it is hard to measure and derive the lumped disturbances directly. As a result, the usage of the robust PFC with disturbances is a challenging work. In order to settle this problem, the nonlinear disturbance observer (NDO) is introduced to estimate the lumped disturbances in this section.

Considering the lumped disturbances with (3), the nonlinear dynamic model for the flight vehicle with (1) can also be rewritten as

$$\begin{aligned} \dot{\mathbf{x}} &= \mathbf{f}\left(\mathbf{x}\right) + \mathbf{g}\left(\mathbf{x}\right)u + \mathbf{d}, \\ \mathbf{y} &= \mathbf{C}\mathbf{x}, \end{aligned} \tag{22}$$

where

$$\begin{aligned} \mathbf{x} &= \left[\alpha \;\; q \;\; \delta\right]^T, \\ \mathbf{f}\left(\mathbf{x}\right) &= \begin{bmatrix} f_1\left(\alpha\right) + q + b_1\left(\alpha\right)\delta \\ f_2\left(\alpha\right) + b_2\delta \\ \dfrac{-\delta}{\tau} \end{bmatrix}, \\ \mathbf{g}\left(\mathbf{x}\right) &= \begin{bmatrix} 0 & 0 & \dfrac{1}{\tau} \end{bmatrix}^T. \end{aligned} \tag{23}$$

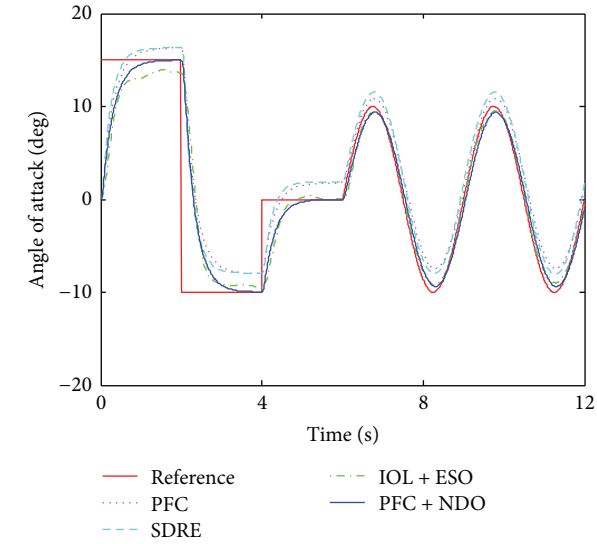

(a) Angle of attack (deg)

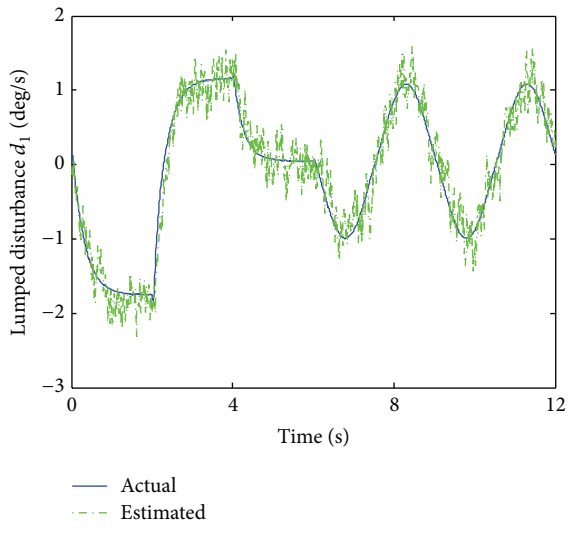

(b) Lumped disturbance d_1 (deg/s)

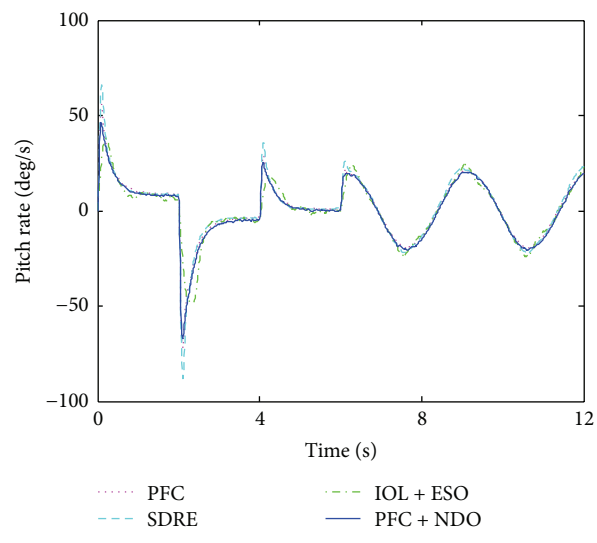

(c) Pitch rate (deg/s)

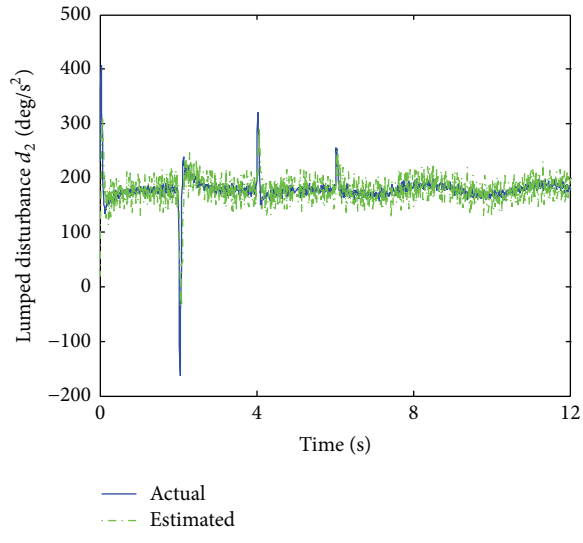

(d) Lumped disturbance d_2 (deg/s^2)

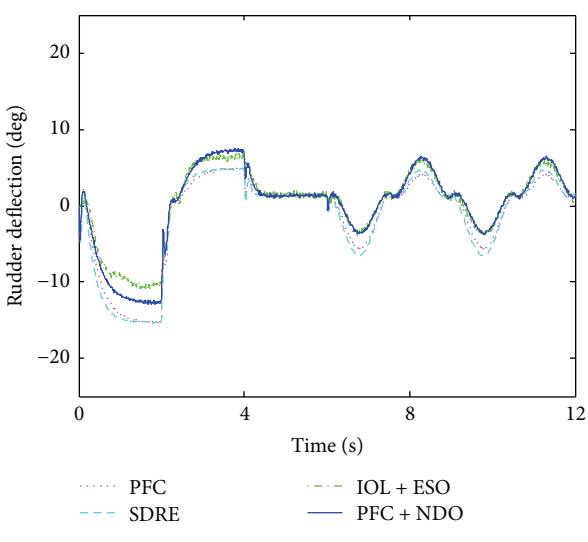

(e) Rudder deflection (deg)

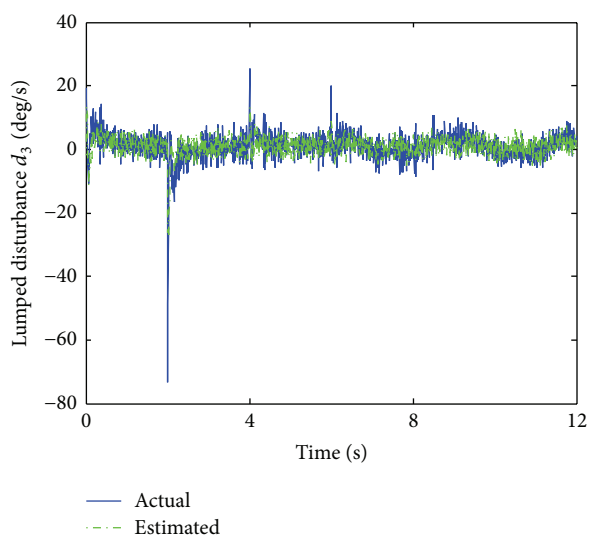

(f) Lumped disturbance d_3 (deg/s)

Figure 4: Continued.

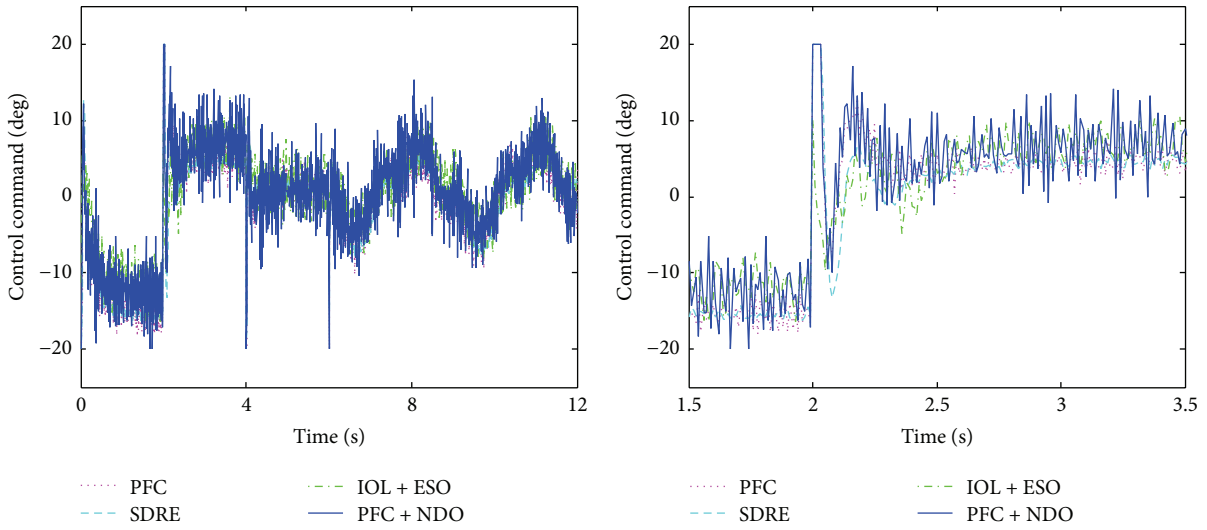

(g) Control command (deg)

(h) Control command (partial section) (deg)

Figure 4: Simulation responses under the four controllers and the estimate performance of the NDO with measurement noise in the case of positive uncertainties and disturbances.

In this case, the NDO is used to estimate the lumped disturbance $\mathbf{d}$, given by

$$\begin{aligned} \dot{\mathbf{z}} &= -\mathbf{l}(\mathbf{x})\,\mathbf{z} - \mathbf{l}(\mathbf{x})\left[\mathbf{f}(\mathbf{x}) + \mathbf{g}(\mathbf{x})\,u + \mathbf{p}(\mathbf{x})\right], \\ \hat{\mathbf{d}} &= \mathbf{z} + \mathbf{p}(\mathbf{x}), \end{aligned} \tag{24}$$

where $\mathbf{z}$ is the internal state of the NDO and $\hat{\mathbf{d}}$ is the system output, which is also the estimate of the lumped disturbance. The nonlinear observer gain $\mathbf{l}(\mathbf{x})$ is defined as

$$\mathbf{l}(\mathbf{x}) = \frac{\partial \mathbf{p}(\mathbf{x})}{\partial \mathbf{x}}, \tag{25}$$

where $\mathbf{p}(\mathbf{x})$ is a nonlinear function to be designed.

Define the estimated error of the lumped disturbance as $\mathbf{e} = \hat{\mathbf{d}} - \mathbf{d}$, and the estimated error dynamic of the NDO is then represented as

$$\dot{\mathbf{e}} = -\mathbf{l}(\mathbf{x})\,\mathbf{e} - \dot{\mathbf{d}}. \tag{26}$$

When $\mathbf{p}(\mathbf{x})$ is chosen such that $\dot{\mathbf{e}} = -\mathbf{l}(\mathbf{x})\mathbf{e}$ is globally exponentially stable, and the derivation of the lumped disturbance $\dot{\mathbf{d}}$ is bounded, the estimated error dynamic of the NDO is bounded stability according to Lemma 4.6 in [35].

Remark 2. Supposing that the lumped disturbance $\mathbf{d}$ is constant, that is, $\dot{\mathbf{d}} = \mathbf{0}$, which may be satisfied when the designed dynamic model is almost identical with the actual model and the external disturbances are constant, it is evident that the estimated error dynamic is asymptotically stable, and the estimated error of the NDO is asymptotically convergent towards zero.

Therefore, the robust predictive functional control based on nonlinear disturbance observer is deduced by substituting the estimated $\hat{\mathbf{d}}$ for the lumped disturbance $\mathbf{d}$ in (21). The framework of the robust PFC is illustrated in Figure 1.

In each control period, the NDO estimates the lumped disturbances using the state and control signals, and then the robust PFC with disturbances optimizes the predictive tracking error of the system. As the control signal is structured as a linear prespecified combination of base functions, the analytic optimal control can be derived. Therefore, the robust PFC can calculate the control signal online via just finite algebraic operations in real time, which is an essential factor for the flight control system.

4. Simulation Results

Compared with the PI and SDRE flight control methods, the effectiveness and robustness of the PFC were validated in [18]. In addition, [8] verified the efficacy of the input-output linearization (IOL) control based on extended state observer (namely, IOL + ESO) in comparison with IOL, MPC, and SMC. Therefore, to demonstrate the tracking performance of the proposed method, the simulation results of the four controllers, such as PFC, SDRE, IOL + ESO, and the proposed robust PFC (namely, PFC + NDO), are illustrated under various conditions in succession.

The desired angle of attack is supposed as a combination of square and sine signals, designed as

$$\alpha_c = \begin{cases} 15, & t < 2\,\mathrm{s} \\ -10, & t < 4\,\mathrm{s} \\ 0, & t < 6\,\mathrm{s} \\ 10\sin(2\pi f t), & t \geq 6\,\mathrm{s}, \end{cases} \tag{27}$$

where $f = 1/3$ Hz is the frequency of the sine signal.

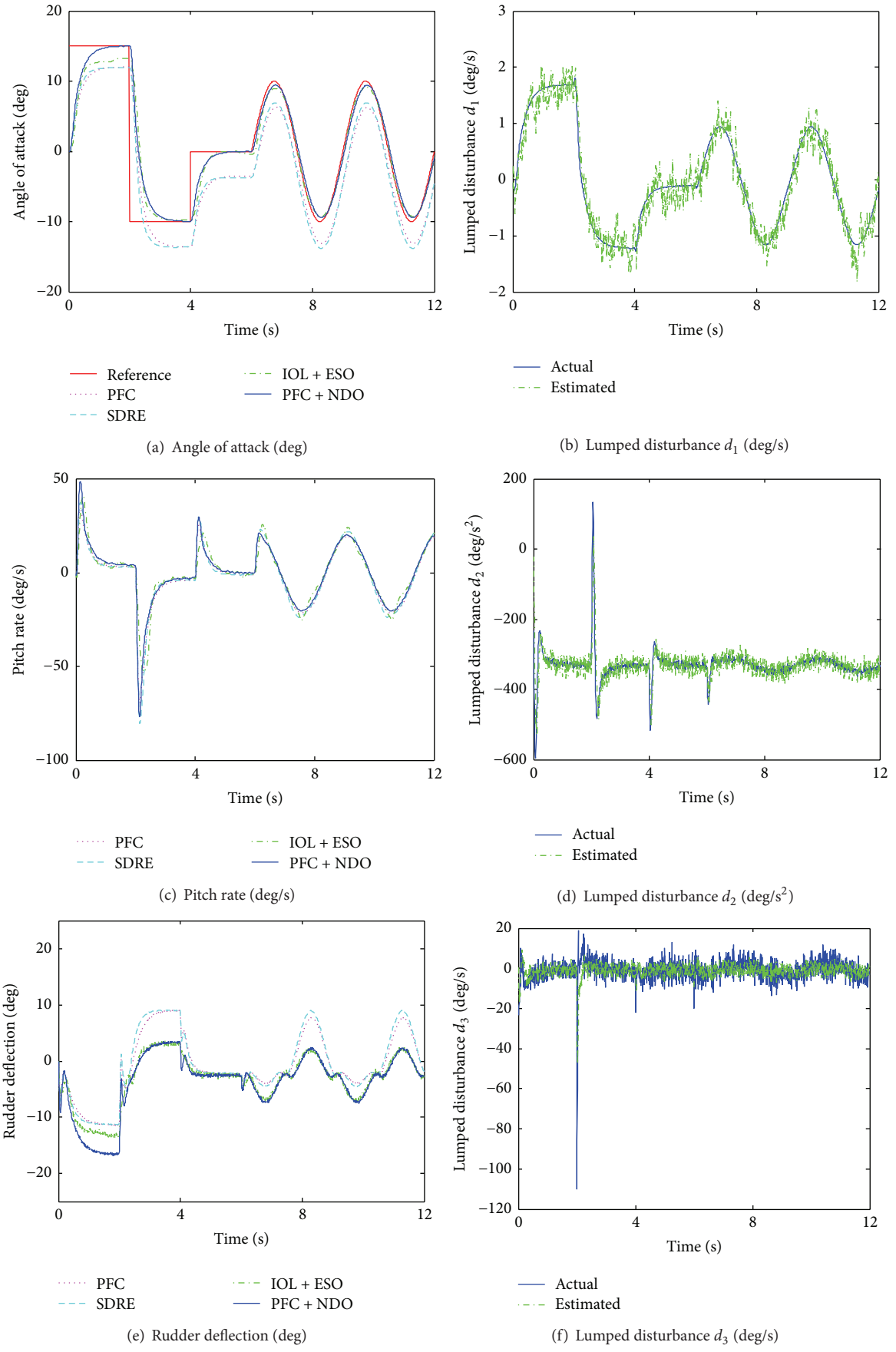

(a) Angle of attack (deg)

(b) Lumped disturbance d_1 (deg/s)

(c) Pitch rate (deg/s)

(d) Lumped disturbance d_2 (deg/s^2)

(e) Rudder deflection (deg)

(f) Lumped disturbance d_3 (deg/s)

Figure 5: Continued.

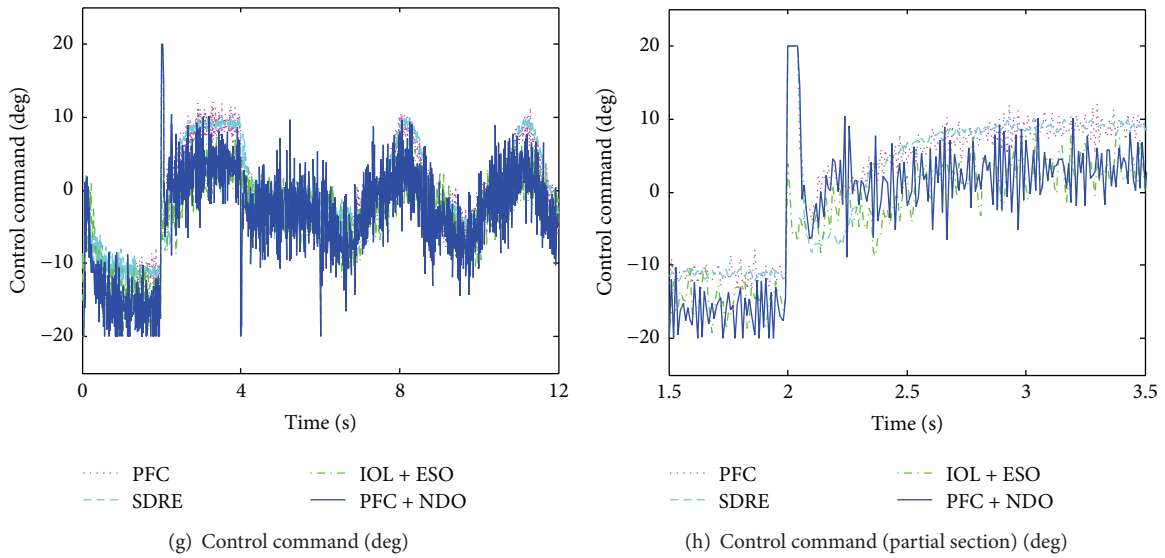

(g) Control command (deg) (h) Control command (partial section) (deg)

FIGURE 5: Simulation responses under the four controllers and the estimate performance of the NDO with measurement noise in the case of negative uncertainties and disturbances.

The hard limits imposed on the servo are ±20 deg for its deflection and ±250 deg/s for its rate of change, respectively. Thus, the soft limit of the control command is ±20 deg for its magnitude.

Moreover, a number of simulations are carried out to determine the controller parameters. In the SDRE, the weighting matrices are selected as $\mathbf{Q} = \text{diag}\,[100 \;\; 4 \;\; 1]$, $r = 10$, and the algebraic Riccati equation is solved in real-time with Schur algorithm. In the IOL + ESO, the bandwidth of the IOL is selected as 10 Hz, whereas the bandwidth of the ESO is 100 Hz. In PFC, the base function is designed as $f_1(\cdot) = 1$, the settling time of the reference trajectory is $T_r = 0.2$ s, and the set of the coincidence point in the performance index is $H_{N_c} = \{7 \;\; 8\}$. When it comes to the NDOEPFCNDO, the parameters of the PFC part are identical to the PFC, the nonlinear function is designed as $\mathbf{p}(\mathbf{x}) = [\omega_\alpha \alpha \;\; \omega_q q \;\; \omega_\delta \delta]^T$, and then the nonlinear observer gain $\mathbf{l}(\mathbf{x}) = \text{diag}\,[\omega_\alpha \;\; \omega_q \;\; \omega_\delta]$ is a diagonal matrix, where $\omega_\alpha = 20$, $\omega_q = 30$, and $\omega_\delta = 40$. For all of the flight controllers, the control period is given by 0.01 s.

4.1. Parameter Uncertainties and External Disturbances. In this simulation, the parameter uncertainties and external disturbances are considered. The uncertainty ranges of the flight vehicle model are set as aerodynamic coefficients uncertainty within ±30% and servo time constant uncertainty within ±10%. Simultaneously, the external disturbance bounds of the channel of angle of attack and pitch rate are supposed to be ±0.0686 deg/s and ±232 deg/s^2, respectively, which means that the bounds of the external disturbed force and moment are assumed to be ±5000 N and ±1000 Nm individually. Moreover, the external disturbance limitation of the servo channel is considered as ±1 deg/s.

The response curves of all variables of the flight vehicle are shown in Figures 2 and 3, and all the uncertainties and disturbances are positive in Figure 2 and negative in Figure 3. It can be seen from Figures 2(a) and 3(a) that whether the uncertainties and disturbances are all positive or negative, both the proposed PFC + NDO and the IOL + ESO methods can achieve excellent tracking performance, whereas both PFC and SDRE behave poorly with a certain constant shift. As illustrated in Figures 2(g), 2(h), 3(g), and 3(h), when the system is stable, the control commands of the SDRE and PFC have a certain offset compared with the other two controllers, which indicates that some external disturbances imposed on the system cannot be detected or compensated in the PFC, which results in the static error of these two methods. However, the lumped disturbances are estimated by the NDO as presented in Figures 2(b), 2(d), 2(f), 3(b), 3(d), and 3(f) in the PFC + NDO approach. Although it is relatively large when the desired angle of attack has a sudden change, the estimated error of the NDO is rather slight in the whole flight envelop, which guarantees the robustness of the proposed approaches.

4.2. Measurement Noise. Besides the parameter uncertainties and disturbances, the measurement noise is also a crucial element to be considered for the flight control system design. Based on the above discussion, the angle of attack tracking performance is validated taking the measurement noise into account in this simulation.

Suppose that a zero mean 0.1 deg standard deviation white noise with 0.01 s sample time is disrupted into the measurement of angle of attack and rudder deflection, and a zero mean 1 deg standard deviation white noise with 0.01 s sample time is mixed with the measurement of pitch rate. Meanwhile, as it is demonstrated that the IOL + ESO could be with poor tracking performance, or even unstable under measurement noise, a zero mean 0.01 deg standard deviation white noise, a tenth of the other controllers, is added in angle of attack for this approach.

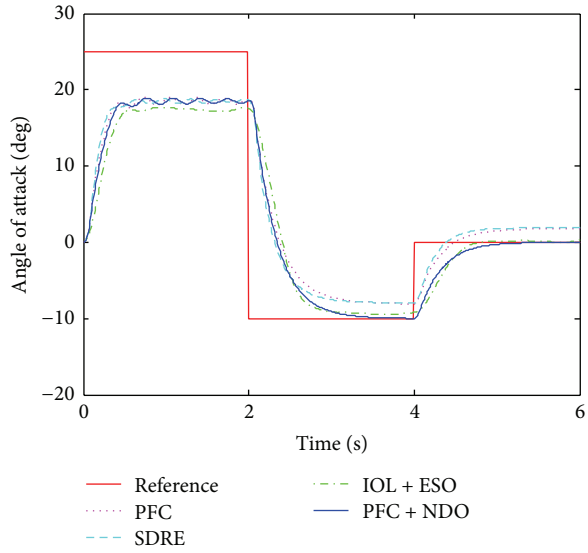

(a) Angle of attack (deg)

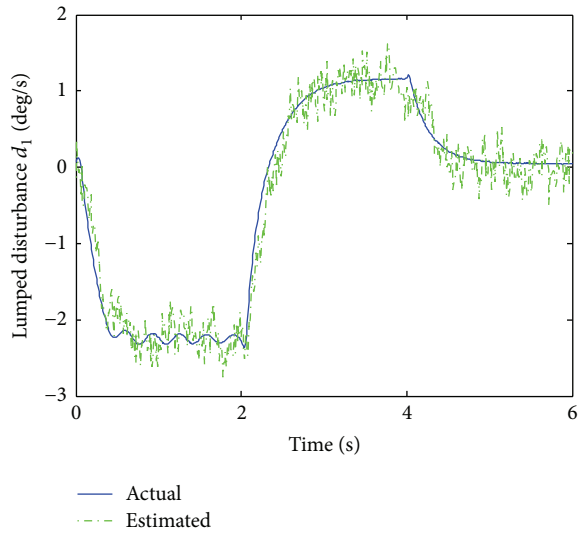

(b) Lumped disturbance d_1 (deg/s)

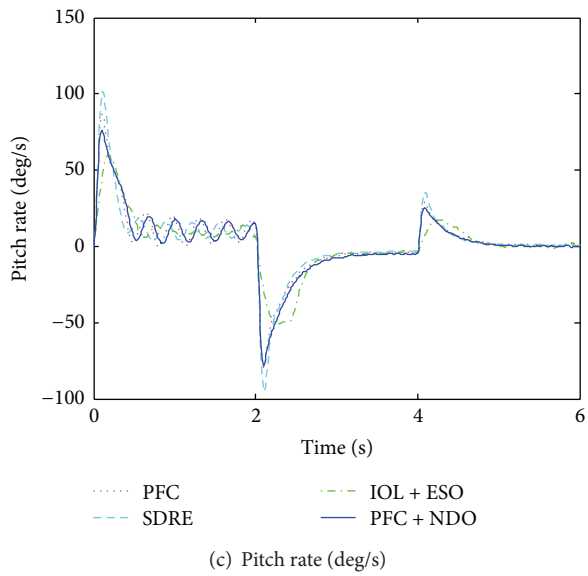

(c) Pitch rate (deg/s)

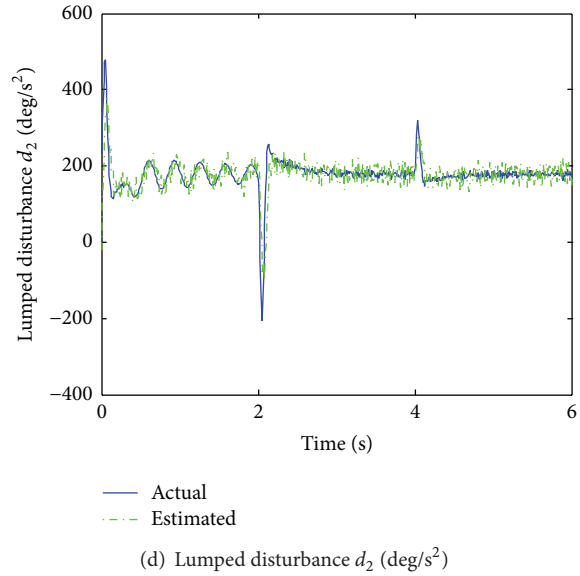

(d) Lumped disturbance d_2 (deg/s^2)

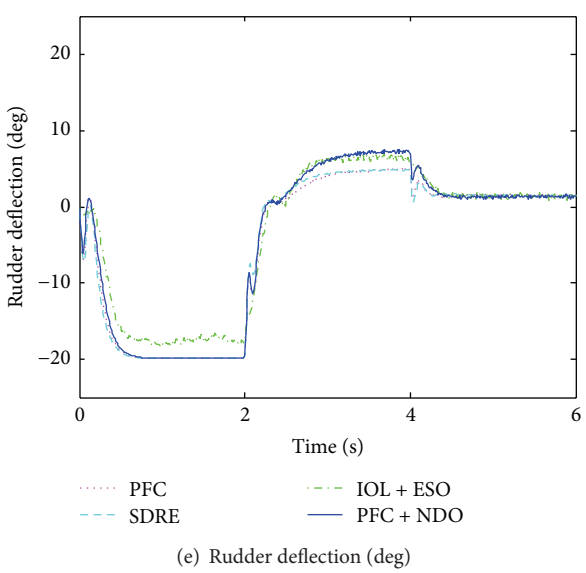

(e) Rudder deflection (deg)

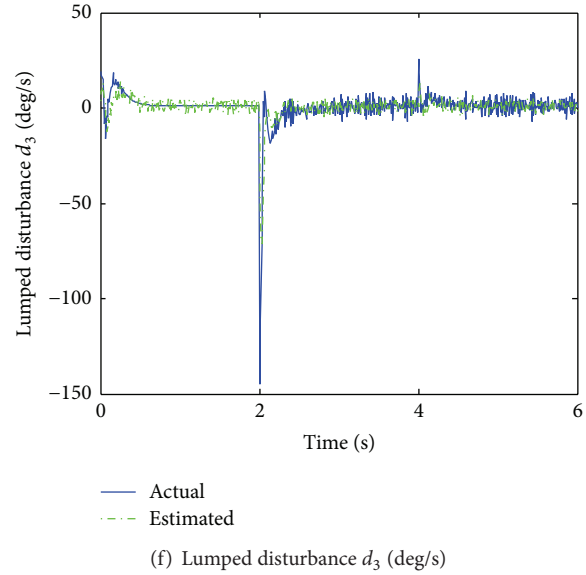

(f) Lumped disturbance d_3 (deg/s)

Figure 6: Continued.

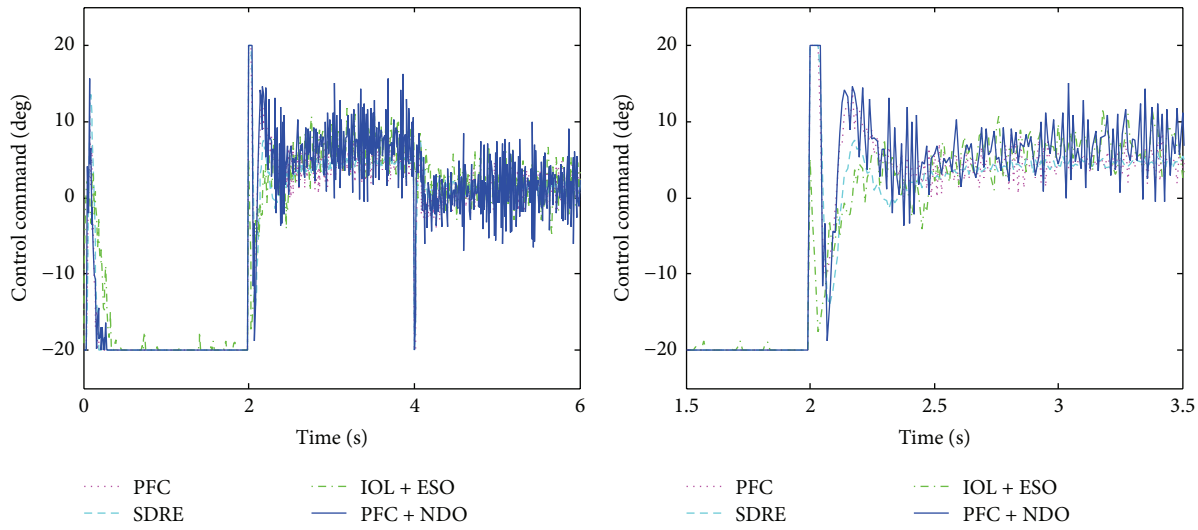

(g) Control command (deg) (h) Control command (partial section) (deg)

Figure 6: Simulation responses of saturation and the estimate performance of the NDO with measurement noise in the case of positive uncertainties and disturbances.

The simulation results are shown in Figures 4 and 5, and all the uncertainties and disturbances are positive in Figure 4 and negative in Figure 5. It is illustrated that both SDRE and PFC are apparently still unable to track the desired angle of attack but insensitive to the measurement noise. Whereas, even with slight measurement noise, the tracking performance of the IOL + ESO decreases quickly especially at the beginning of control, then the control command becomes increasingly vibrational as depicted in Figures 4(g), 4(h), 5(g), and 5(h). In contrast to the former three controllers, the PFC + NDO flight controller demonstrates not only accurate tracking capability but also strong robustness to the parameter uncertainties, external disturbances, and measurement noise. As shown in Figures 4(b), 4(d), 4(f), 5(b), 5(d), and 5(f), the NDO estimated performance of lumped disturbances decreases slightly due to the effect of the measurement noise. Since the estimated lumped disturbances are oscillatory around the actual value, and the measurement noise just increases the magnitude of the oscillation, the PFC + NDO can still estimate and attenuate the lumped disturbances as time passed.

4.3. Control Saturation. To further validate the control performance of the proposed method, the phenomenon of control saturation, which may occur when the desired angle of attack excesses the capability of the actuator due to the high maneuverability of the target, is considered. Therefore, the desired angle of attack is given by

$$\alpha_c = \begin{cases} 25, & t < 2\,\text{s} \\ -10, & t < 4\,\text{s} \\ 0, & t \geq 4\,\text{s}. \end{cases} \tag{28}$$

The simulation results are presented in Figures 6 and 7, and all the uncertainties and disturbances are positive in Figure 6 and negative in Figure 7. From Figures 6(g), 6(h), 7(g), and 7(h), it is observed that when the desired angle of attack increases to 25 deg, the control command reaches saturation, and all of the controllers cannot achieve efficient tracking performance as shown in Figures 6(a) and 7(a). Once the desired angle of attack changes to −10 deg within the capability of control, the proposed robust PFC + NDO method can respond rapidly and recover its effective and robust tracking performance, whereas the SDRE and PFC methods remain unable to compensate the disturbances. Although the IOL + ESO method can recover its tracking performance, the sensitivity to measurement noise significantly prevents this approach from being used in practice.

5. Conclusions

Considering parameter uncertainties, external disturbances, and measurement noise, a novel robust PFC flight control approach based on NDO has been investigated. With the assistance of the NDO, the proposed robust PFC not only inherits the merit from the traditional PFC, but also possesses the ability of matched and mismatched disturbance attenuation. Consequently, the tracking performance of the robust PFC indicates a considerable improvement. A comparison of the proposed design with the other flight control in the literature has been carried out, and the superiority of the proposed design in terms of robustness and effectiveness has been clearly verified. Since the boundary information of the uncertainties and disturbances is not indispensable, together with its insusceptibility to measurement noise, the robust PFC flight control has potential to be a considerably promising candidate to be used in engineering practice, which will be validated afterwards.

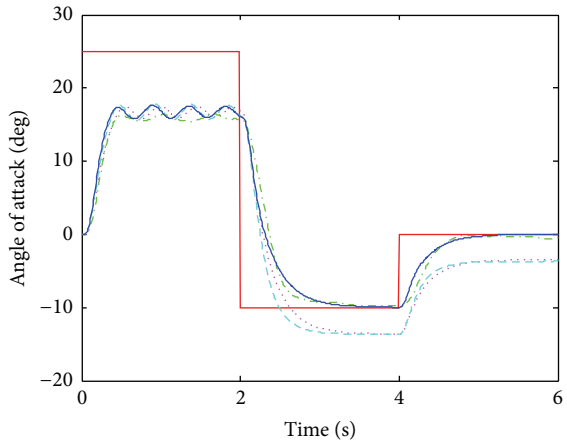

(a) Angle of attack (deg)

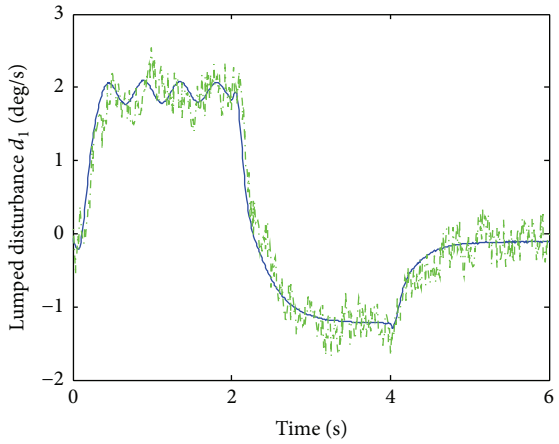

(b) Lumped disturbance d_1 (deg/s)

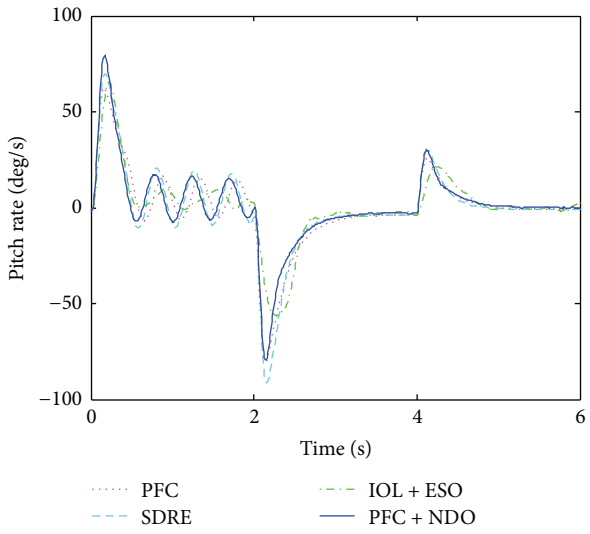

(c) Pitch rate (deg/s)

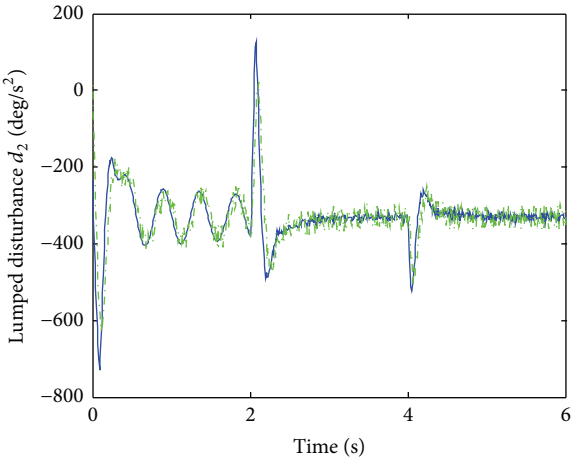

(d) Lumped disturbance d_2 (deg/s^2)

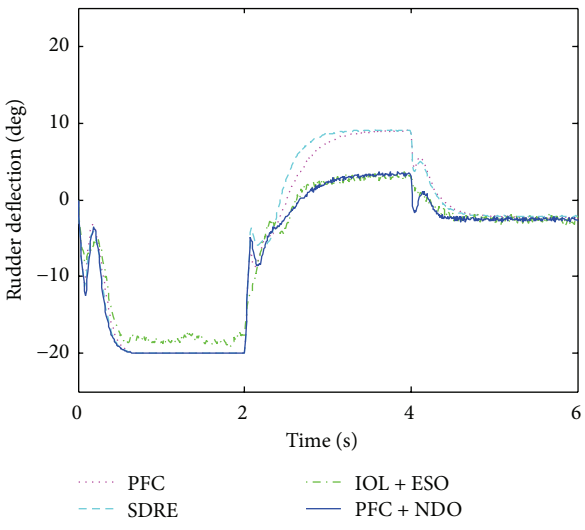

(e) Rudder deflection (deg)

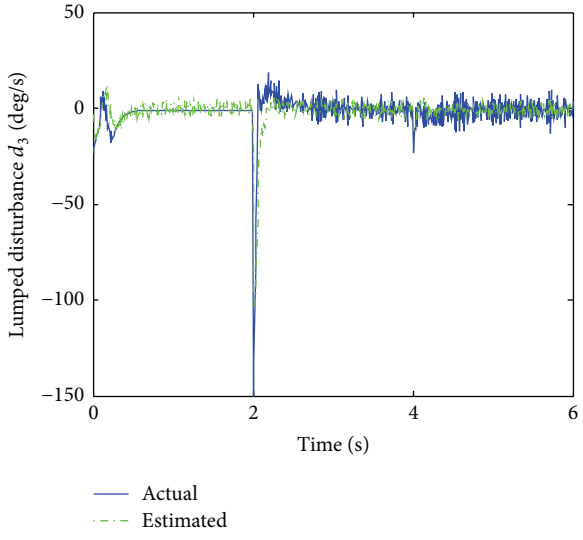

(f) Lumped disturbance d_3 (deg/s)

Figure 7: Continued.

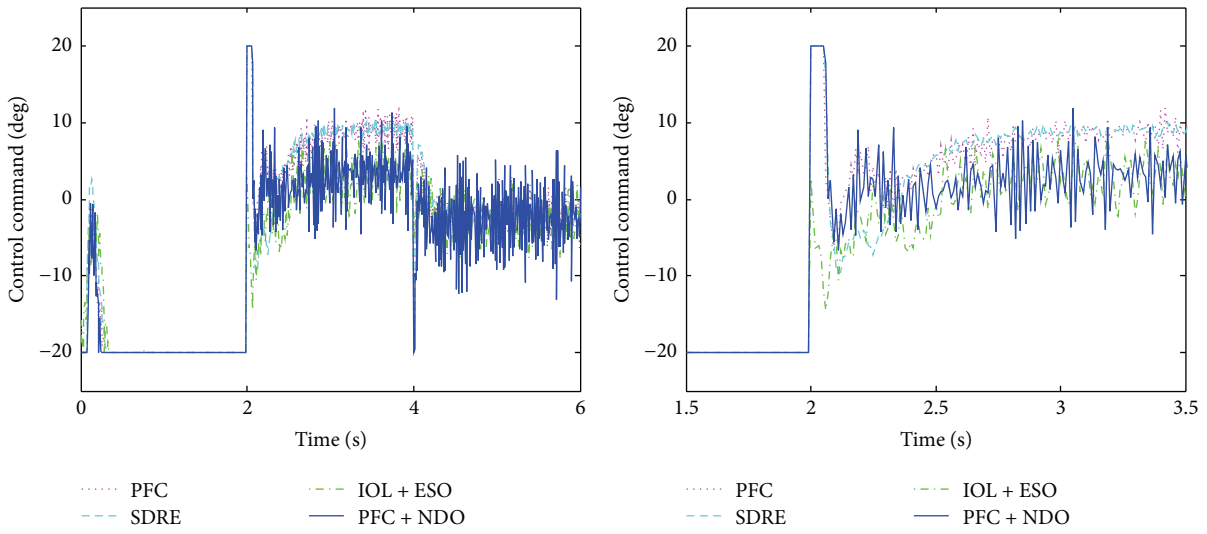

(g) Control command (deg)

(h) Control command (partial section) (deg)

FIGURE 7: Simulation responses of saturation and the estimate performance of the NDO with measurement noise in the case of negative uncertainties and disturbances.

Conflict of Interests

There is no conflict of interests regarding the publication of this paper.

References

[1] M. P. Horton, "Autopilots for tactical missiles: an overview," *Proceedings of the Institution of Mechanical Engineers. Part I, Journal of systems and control engineering*, vol. 209, no. 2, pp. 127–139, 1995.

[2] H. Buschek, "Full envelope missile autopilot design using gain scheduled robust control," *Journal of Guidance, Control, and Dynamics*, vol. 22, no. 1, pp. 115–122, 1999.

[3] E. Devaud, H. Siguerdidjane, and S. Font, "Some control strategies for a high-angle-of-attack missile autopilot," *Control Engineering Practice*, vol. 8, no. 8, pp. 885–892, 2000.

[4] E. Devaud, J.-P. Harcaut, and H. Siguerdidjane, "Three-axes missile autopilot design: from linear to nonlinear control strategies," *Journal of Guidance, Control, and Dynamics*, vol. 24, no. 1, pp. 64–71, 2001.

[5] S. Theodoulis and G. Duc, "Gain scheduled autopilot synthesis for an atmosphere re-entry vehicle," in *Proceedings of the AIAA Guidance, Navigation and Control Conference and Exhibit*, Honolulu, Hawaii, USA, August 2008.

[6] B. A. White, L. Bruyere, and A. Tsourdos, "Missile autopilot design using quasi-LPV polynomial eigenstructure assignment," *IEEE Transactions on Aerospace and Electronic Systems*, vol. 43, no. 4, pp. 1470–1483, 2007.

[7] Y. Kim and B. S. Kim, "Pitch autopilot design for agile missiles with uncertain aerodynamic coefficients," *IEEE Transactions on Aerospace and Electronic Systems*, vol. 49, no. 2, pp. 907–914, 2013.

[8] A. A. Godbole, T. R. Libin, and S. E. Talole, "Extended state observer-based robust pitch autopilot design for tactical missiles," *Proceedings of the Institution of Mechanical Engineers, Part G: Journal of Aerospace Engineering*, vol. 226, no. 12, pp. 1482–1501, 2012.

[9] I. Yang, D. Kim, and D. Lee, "A flight control strategy using robust dynamic inversion based on sliding mode control," in *AIAA Guidance, Navigation, and Control Conference*, The American Institute of Aeronautics and Astronautic, Minneapolis, Minn, USA, 2012.

[10] T. Shima, M. Idan, and O. M. Golan, "Sliding-mode control for integrated missile autopilot guidance," *Journal of Guidance, Control, and Dynamics*, vol. 29, no. 2, pp. 250–260, 2006.

[11] G. Mattei and S. Monaco, "Nonlinear autopilot design for an asymmetric missile using robust backstepping control," *Journal of Guidance, Control, and Dynamics*, vol. 37, no. 5, pp. 1462–1476, 2014.

[12] G. Mattei and S. Monaco, "Nonlinear robust autopilot for rolling and lateral motions of an aerodynamic missile," in *Proceedings of the AIAA Guidance, Navigation, and Control Conference*, Minneapolis, Minn, USA, 2012.

[13] S.-H. Kim, Y.-S. Kim, and C. Song, "A robust adaptive nonlinear control approach to missile autopilot design," *Control Engineering Practice*, vol. 12, no. 2, pp. 149–154, 2004.

[14] F. Peter, F. Holzapfel, E. Xargay, and N. Hovakimyan, "L1 Adaptive augmentation of a missile autopilot," in *Proceedings of the AIAA Guidance, Navigation, and Control Conference*, Minneapolis, Minn, USA, 2012.

[15] I. Barkana, "Simple adaptive control for non-minimum phase autopilot design," in *Proceedings of the AIAA Guidance, Navigation, and Control Conference*, pp. 511–522, Providence, RI, USA, August 2004.

[16] T. Satoh, K. Kaneko, and N. Saito, "Performance improvement of predictive functional control: a disturbance observer approach," in *Proceedings of the 37th Annual Conference of the IEEE Industrial Electronics Society (IECON '11)*, pp. 669–674, Melbourne, VIC, Australia, November 2011.

[17] D. Dovžan and I. Škrjanc, "Predictive functional control based on an adaptive fuzzy model of a hybrid semi-batch reactor," *Control Engineering Practice*, vol. 18, no. 8, pp. 979–989, 2010.

[18] W.-Q. Tang and Y.-L. Cai, "Predictive functional control-based missile autopilot design," *Journal of Guidance, Control, and Dynamics*, vol. 35, no. 5, pp. 1450–1455, 2012.

[19] A. Vivas and P. Poignet, "Predictive functional control of a parallel robot," *Control Engineering Practice*, vol. 13, no. 7, pp. 863–874, 2005.

[20] H. Liu and S. Li, "Speed control for PMSM servo system using predictive functional control and extended state observer," *IEEE Transactions on Industrial Electronics*, vol. 59, no. 2, pp. 1171–1183, 2012.

[21] M. Lepetič, I. Škrjanc, H. G. Chiacchiarini, and D. Matko, "Predictive functional control based on fuzzy model: comparison with linear predictive functional control and PID control," *Journal of Intelligent and Robotic Systems: Theory and Applications*, vol. 36, no. 4, pp. 467–480, 2003.

[22] I. Škrjanc and S. Blažič, "Predictive functional control based on fuzzy model: design and stability study," *Journal of Intelligent and Robotic Systems: Theory and Applications*, vol. 43, no. 2–4, pp. 283–299, 2005.

[23] K. Youcef-Toumi and O. Ito, "Time delay controller for systems with unknown dynamics," *Journal of Dynamic Systems, Measurement and Control, Transactions of the ASME*, vol. 112, no. 1, pp. 133–142, 1990.

[24] Q.-C. Zhong and D. Rees, "Control of uncertain LTI systems based on an uncertainty and disturbance estimator," *Journal of Dynamic Systems, Measurement and Control*, vol. 126, no. 4, pp. 905–910, 2004.

[25] J. Han, *Active Disturbance Rejection Control Technique—The Technique for Estimating and Compensating the Uncertainties*, National Defense Industry Press, Beijing, China, 2009.

[26] W.-H. Chen, "Nonlinear disturbance observer-enhanced dynamic inversion control of missiles," *Journal of Guidance, Control, and Dynamics*, vol. 26, no. 1, pp. 161–166, 2003.

[27] H. Lee, X. Huang, and H. Yin, "Enhanced sliding mode control for missile autopilot based on nonlinear disturbance observer," in *Proceedings of the International Joint Conference on Computational Sciences and Optimization (CSO '09)*, pp. 210–213, April 2009.

[28] J. Yang, W.-H. Chen, and S. Li, "Non-linear disturbance observer-based robust control for systems with mismatched disturbances/uncertainties," *IET Control Theory & Applications*, vol. 5, no. 18, pp. 2053–2062, 2011.

[29] W. Chen, D. Balance, P. Gawthrop, J. Gribble, and J. O'Reilly, "Nonlinear PID predictive controller," *IEE Proceedings: Control Theory and Applications*, vol. 146, no. 6, pp. 603–611, 1999.

[30] R. Errouissi, M. Ouhrouche, and W.-H. Chen, "Robust nonlinear generalized predictive control of a permanent magnet synchronous motor with an anti-windup compensator," in *Proceedings of the IEEE International Symposium on Industrial Electronics (ISIE '10)*, pp. 3184–3189, IEEE, Bari, Italy, July 2010.

[31] S. Li, J. Yang, W.-H. Chen, and X. Chen, "Generalized extended state observer based control for systems with mismatched uncertainties," *IEEE Transactions on Industrial Electronics*, vol. 59, no. 12, pp. 4792–4802, 2012.

[32] J. Yang, S. Li, and X. Yu, "Sliding-mode control for systems with mismatched uncertainties via a disturbance observer," *IEEE Transactions on Industrial Electronics*, vol. 60, no. 1, pp. 160–169, 2013.

[33] R. T. Reichert, "Dynamic scheduling of modern-robust-control autopilot designs for missiles," *IEEE Control Systems*, vol. 12, no. 5, pp. 35–42, 1992.

[34] J. M. Maciejowski, *Predictive Control with Constraints*, Prentice-Hall, Upper Saddle River, NJ, USA, 2002.

[35] H. Khalil, *Nonlinear Systems*, Prentice-Hall, Upper Saddle River, NJ, USA, 3rd edition, 2002.